

# Classification of the charged test particle circular orbits in Reissner–Nordström spacetime

Daniela Pugliese<sup>1</sup>, Hernando Quevedo<sup>2,3,4</sup>, and Remo Ruffini<sup>2</sup>

<sup>1</sup> School of Mathematical Sciences, Queen Mary, University of London, Mile End Road, London E1 4NS, United Kingdom

<sup>2</sup> Dipartimento di Fisica and ICRA, Università di Roma “La Sapienza”, Piazzale Aldo Moro 5, I-00185 Roma, Italy  
ICRANet, Piazzale della Repubblica 10, I-65122 Pescara, Italy

<sup>3</sup> Instituto de Ciencias Nucleares, Universidad Nacional Autónoma de México, AP 70543, México, DF 04510, Mexico

<sup>4</sup> Instituto de Cosmologia, Relatividade e Astrofisica and ICRANet - CBPF  
Rua Dr. Xavier Sigaud, 150, CEP 22290-180, Rio de Janeiro, Brazil

E-mail: d.pugliese.physics@gmail.com, quevedo@nucleares.unam.mx, ruffini@icra.it

**Abstract.** We study the circular motion of charged test particles in the gravitational field of a charged mass described by the Reissner–Nordström spacetime, focusing on the physical differences between black holes and naked singularities. We perform the most complete classification of circular orbits for different sets of the main physical parameters, and study numerically the behavior of the angular momentum and energy of the charged test particle. Our analysis shows in an alternative manner that the behavior of circular orbits can be used to distinguish between black holes and naked singularities.

PACS numbers: 04.20.-q, 04.70.Bw, 04.40.Dg

## 1. Introduction

The Reissner–Nordström (RN) line element

$$ds^2 = -\frac{\Delta}{r^2} dt^2 + \frac{r^2}{\Delta} dr^2 + r^2 (d\theta^2 + \sin^2 \theta d\phi^2) , \quad (1)$$

in standard spherical coordinates, describes the background of a static gravitational source of mass  $M$  and charge  $Q$ , where  $\Delta = (r - r_+)(r - r_-)$  and  $r_{\pm} = M \pm \sqrt{M^2 - Q^2}$  are the radii of the outer and inner horizon, respectively.

The motion of a test particle of charge  $q$  and mass  $\mu$  moving in a RN background (1) is described by the following Lagrangian density:

$$\mathcal{L} = \frac{1}{2} g_{\alpha\beta} \dot{x}^\alpha \dot{x}^\beta + \epsilon A_\alpha \dot{x}^\alpha , \quad (2)$$

where  $A_\alpha$  are the components of the electromagnetic 4-potential, the dot represents differentiation with respect to the proper time, and the parameter  $\epsilon = q/\mu$  is the specific charge of the test particle.

Since the Lagrangian density (2) does not depend explicitly on the variables  $t$  and  $\phi$ , the following two conserved quantities exist

$$p_t \equiv \frac{\partial \mathcal{L}}{\partial \dot{t}} = - \left( \frac{\Delta}{r^2} \dot{t} + \frac{\epsilon Q}{r} \right) = - \frac{E}{\mu}, \quad (3)$$

$$p_\phi = \frac{\partial \mathcal{L}}{\partial \dot{\phi}} = r^2 \sin^2 \theta \dot{\phi} = \frac{L}{\mu}, \quad (4)$$

where  $L$  and  $E$  are respectively the angular momentum and energy of the particle as measured by an observer at rest at infinity.

On the equatorial plane  $\theta = \pi/2$ , the motion equations can be reduced to the form  $\dot{r}^2 + V^2 = E^2/\mu^2$  which describes the motion of a test particle inside an effective potential  $V$ . Then, it is convenient to define the potential

$$V_\pm = \frac{E_\pm}{\mu} = \frac{\epsilon Q}{r} \pm \sqrt{\left(1 + \frac{L^2}{\mu^2 r^2}\right) \left(1 - \frac{2M}{r} + \frac{Q^2}{r^2}\right)} \quad (5)$$

which corresponds to the value of  $E/\mu$  at which the (radial) kinetic energy of the particle vanishes [1, 2, 3, 4], i. e. it is the value at which  $r$  is a ‘‘turning point’’ ( $V = E/\mu$ ). The effective potential with positive (negative) sign corresponds to the solution with

$$\lim_{r \rightarrow \infty} E_\pm = \pm \mu.$$

Notice that in general  $E_+ \geq E_-$  and  $E_+(L, \epsilon, r) = -E_-(L, -\epsilon, r)$ .

In the limiting case of vanishing charge, the effective potential reduces to

$$V = + \sqrt{\left(1 + \frac{L^2}{\mu^2 r^2}\right) \left(1 - \frac{2M}{r} + \frac{Q^2}{r^2}\right)}. \quad (6)$$

This case was analyzed previously in [5, 6]. In this work, we first found that the stability properties of neutral test particles strongly depend on the nature of the central source. Indeed, in the case of a RN black hole there exists a minimum radius at which the orbit is stable, and outside this radius all the orbits are stable so that there exists only one region of stability. In the case of a naked singularity, the situation is completely different; the region of stability splits into two nonconnected regions so that a zone appears inside which no stable circular orbit can exist. This means that the stability properties of circular orbits could, in principle, be used to differentiate between a black hole and a naked singularity.

In the general case of charged test particles, the presence of the additional term  $\frac{\epsilon Q}{r}$  changes completely the behavior of circular orbits, and leads to several possibilities which must be analyzed separately for black holes and naked singularities. In particular, it turns out that even in the case of the positive solution  $E_+$  and  $\epsilon Q < 0$ , negative energy states can exist [7] and also [8, 9, 10, 11, 12, 13, 14]. In [15], we studied the spatial regions where circular motion is allowed around either black holes or naked singularities. As an example of the action of repulsive gravity, we found all the circles at which a particle can have vanishing angular momentum. We showed that it is possible to use the geometric structure of stable accretion disks, made of only test particles moving along circular orbits around the central body, to clearly distinguish between black holes and naked singularities (see also [16, 17] and [18, 19]). For a recent discussion on the matter of naked singularity and black hole physics see [20, 21] and [22, 23, 24]. Also, there is extensive literature about particle motion in

the RN background. We refer in particular on [15] and reference therein. More recent generalizations of previous analysis are given in [25] and [26].

In this work, we deepen the analysis performed in [15] in order to obtain the complete classification of circular motion around a RN black hole in section 2 and around a RN naked singularity with  $0 < \epsilon < 1$ , in section 4.1, and with  $-1 < \epsilon < 0$ , in section 4.2. Conclusions close the paper in section (5)

## 2. Circular motion

The effective potential (5) regulates the circular motion of charged test particles. Only the special case of the positive solution  $V_+$  will be considered here in order to be able to compare our results with those obtained in the case of neutral test particles analyzed in [5, 6]. The extrema of the function  $V_+$  defined by the relations

$$\frac{dV_+}{dr} = 0, \quad V_+ = \frac{E_+}{\mu}, \quad (7)$$

determine the radius of circular orbits and the corresponding values of the energy  $E$  and the angular momentum  $L$ . In the following analysis, we drop the subindex (+). Solving (7) with respect to  $L$ , we find the specific angular momentum

$$\frac{(L_{\pm})^2}{\mu^2} = \frac{r^2}{2\Sigma^2} \left[ 2(Mr - Q^2)\Sigma + \epsilon^2 Q^2 \Delta \pm Q\Delta \sqrt{\epsilon^2(4\Sigma + \epsilon^2 Q^2)} \right], \quad (8)$$

of the test particle on a circular orbit of radius  $r$ , where

$$\Sigma \equiv r^2 - 3Mr + 2Q^2, \quad (9)$$

and the corresponding energy:

$$\frac{E_{\pm}}{\mu} = \frac{\epsilon Q}{r} + \frac{\Delta \sqrt{2\Sigma + \epsilon^2 Q^2 \pm Q\sqrt{\epsilon^2(4\Sigma + \epsilon^2 Q^2)}}}{\sqrt{2r|\Sigma|}}. \quad (10)$$

An interesting particular orbit is the one for which the particle is located at rest as seen by an observer at infinity, i.e., with  $L = 0$ . These “orbits” are therefore characterized by the following conditions

$$L = 0, \quad \frac{dV}{dr} = 0. \quad (11)$$

[27]. Solving (11) for  $Q \neq 0$  and  $\epsilon \neq 0$ , we find the following radius

$$r_s^{\pm} \equiv \frac{(\epsilon^2 - 1) Q^2 M}{\epsilon^2 Q^2 - M^2} \pm \sqrt{\frac{\epsilon^2 Q^4 (\epsilon^2 - 1) (M^2 - Q^2)}{(\epsilon^2 Q^2 - M^2)^2}}, \quad (12)$$

which is a generalization of the classical radius  $r_* = Q^2/M$  of a mass  $M$  with charge  $Q$ . A detailed analysis of the behavior of this radius was presented in [15].

## 3. Circular motion around a RN black hole

In this section, we present a classification of the circular orbits around a RN black hole ( $Q \leq M$ ) by using certain values of the parameters  $L$  and  $\epsilon$  which follow from the conditions of circular motion. It can be considered as an alternative classification to that presented in [15], in which the value of the ratio  $Q/M$  plays a central role.

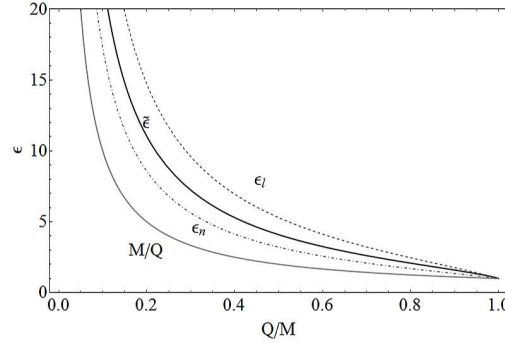


**Figure 1.** The charge parameters  $\epsilon_l$  (dashed curve),  $\tilde{\epsilon}$  (black solid curve),  $\epsilon_n$  (dotted curve), and  $M/Q$  (gray curve) as functions of the charge-to-mass ratio of the RN black hole.

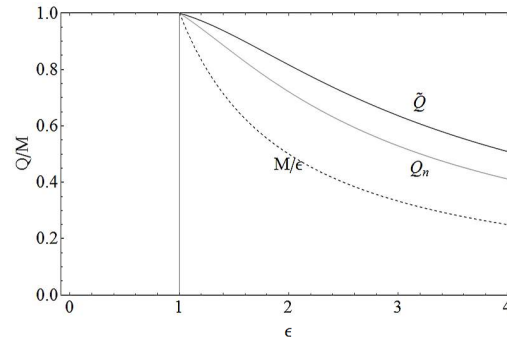


**Figure 2.** The charge parameters  $Q_n$  (gray curve),  $\tilde{Q}$  (black solid curve), and  $M/\epsilon$  (dashed curve) as functions of the charge-to-mass ratio  $\epsilon$  of the test particle.

Here we are interested in the region outside the outer horizon  $r_+$ . Let us introduce the parameters

$$\tilde{\epsilon} \equiv \frac{1}{\sqrt{2}Q} \sqrt{5M^2 - 4Q^2 + \sqrt{25M^2 - 24Q^2}}, \quad (13)$$

$$\epsilon_n \equiv \sqrt{\frac{3M^2}{2Q^2} - 1 + \frac{\sqrt{(9M^2 - 8Q^2)M^2}}{2Q^2}}, \quad (14)$$

$$\tilde{Q} \equiv M \frac{\sqrt{4 + 5\epsilon^2}}{2 + \epsilon^2}, \quad Q_n \equiv M \frac{\sqrt{1 + 3\epsilon^2}}{1 + \epsilon^2}, \quad (15)$$

the behavior of which is depicted in figures 1 and 2.

Moreover, let us introduce the radius

$$r_\gamma^\pm \equiv \frac{3M}{2} \pm \frac{1}{2} \sqrt{9M^2 - 8Q^2}, \quad (16)$$

which represents the limiting radius at which neutral particles can be in circular motion around a RN naked singularity [5], the angular momentum parameter and

$$L_n^2 \equiv \frac{9M^7}{2\epsilon^2 Q^2} \left( 3M + \sqrt{9M^2 - 8Q^2} \right) + \frac{2Q^2 M^2}{\epsilon^2} (1 + \epsilon^2)$$

**Table 1.** Characteristics of the circular orbits for charged test particles with charge-to-mass ratio  $\epsilon \leq 1$  in a RN black hole.

| $0 < \epsilon \leq 1$    |                 | $\epsilon < 0$   |               |
|--------------------------|-----------------|------------------|---------------|
| Region                   | Momentum        | Region           | Momentum      |
| $r = r_l^+$              | $L = \pm L_-$   | $r > r_\gamma^+$ | $L = \pm L_+$ |
| $r_l^+ < r < r_\gamma^+$ | $L = \pm L_\pm$ |                  |               |
| $r = r_\gamma^+$         | $L = \pm L_n$   |                  |               |
| $r > r_\gamma^+$         | $L = \pm L_-$   |                  |               |

$$-\frac{M^3}{2\epsilon^2} \left[ 27M + 5\sqrt{9M^2 - 8Q^2} + 3 \left( 3M + \sqrt{9M^2 - 8Q^2} \right) \epsilon^2 \right], \quad (17)$$

which satisfies the relationship  $(dV/dr)(L_n, r_\gamma^+) = 0$ , and the radius

$$r_l^\pm \equiv \frac{3M}{2} \pm \frac{1}{2} \sqrt{9M^2 - 8Q^2 - Q^2\epsilon^2}, \quad (18)$$

$$(19)$$

where

$$\lim_{\epsilon \rightarrow 0} r_l^\pm = r_\gamma^\pm. \quad (20)$$

We consider separately the two cases  $\epsilon < 1$  and  $\epsilon > 1$  and investigate the value of the allowed orbit's radius and the corresponding angular momentum. The results are summarized for  $\epsilon \leq 1$  in Table 1, and for  $\epsilon > 1$  in Tables 3 and 4. Moreover, the characteristic parameters for all the different cases are listed in Table 2.

We can summarize the results as follows. For  $\epsilon \leq 1$ , Table 1, the infimum circular orbital radius is located at  $r_\gamma^+$  ( $r_l^+$ ) for  $\epsilon < 0$  ( $0 < \epsilon \leq 1$ ). The situation is much more complicated for the case ( $0 < \epsilon \leq 1$ ). In this case, the electromagnetic interaction is repulsive, and is balanced by the attractive gravitational component. Different values of the angular momentum are possible in the set  $\{\pm L_\pm, \pm L_n\}$ . The region in which circular orbits are allowed is therefore split by the radius  $r_\gamma^+$  and  $r_l^+$ .

The case  $\epsilon > 1$  should be considered apart. This corresponds to the real case of charged elementary particles, like electrons, protons and ions, orbiting around a charged source. In the case  $\epsilon Q > 0$  with  $\epsilon > 1$ , the circular motion dynamics is determined by the classification given in 3, for a fixed source charge-to-mass ratio, or in 4, for a fixed particle charge-to-mass ratio.

First, we can recognize nine different situations listed in Table (2). There are orbits with angular momentum  $L = \pm L_\pm$ ,  $L = \pm L_n$  or even  $L = 0$ . This last case occurs when the particle is located at rest with respect to an observer at infinity. Clearly, these particular "orbits" are the consequence of the full balance between the attraction and repulsion among test particles and sources. The infimum circular orbital radius can be  $r = r_\gamma^+$ ,  $r = r_l^+$  or also  $r = r_s^+$ . Comparing with the case  $\epsilon < 1$ , we can clearly see that the main difference between the two cases consists in the presence of a supremum circular orbital radius at  $r = r_\gamma^+$  or at  $r = r_s^+$ . This means that the repulsive electromagnetic effect, predominant at larger distances, does not allow circular orbits around the source. The classifications of Table 3 and Table 4 are alternative and equivalent. In the first one, if we fix the charge-to-mass ratio of the black hole, and we move towards increasing values of the particle charge-to-mass

**Table 2.** Values of the angular momentum  $L$  which are possible in different regions of the radial coordinate  $r$ .

| Case I                 |                      | Case II                                    |                 | Case III              |                 |
|------------------------|----------------------|--|-----------------|-----------------------|-----------------|
| Region                 | Momentum             | Region                                     | Momentum        | Region                | Momentum        |
| $r = r_l^+$            | $L = \pm L_-$        | $r = r_l^+$                                | $L = \pm L_-$   | $r = r_l^+$           | $L = \pm L_-$   |
| $(r_l^+, r_\gamma^+)$  | $L = \pm L_\pm$      | $(r_l^+, r_\gamma^+)$                      | $L = \pm L_\pm$ | $(r_l^+, r_\gamma^+)$ | $L = \pm L_\pm$ |
| $r = r_\gamma^+$       | $L = \pm L_n$        | $r = r_\gamma^+$                           | $L = \pm L_n$   | $r = r_\gamma^+$      | $L = 0$         |
| $(r_\gamma^+, \infty)$ | $L = \pm L_-$        | $(r_\gamma^+, r_s^+)$                      | $L = \pm L_-$   |                       |                 |
| Case IV                |                      | Case V                                     |                 | Case VI               |                 |
| Region                 | Momentum             | Region                                     | Momentum        | Region                | Momentum        |
| $r = r_l^+$            | $L = \pm L_-$        | $r = r_l^+(r_s^+)$                         | $L = 0$         | $r = r_l^+$           | $L = \pm L_-$   |
| $(r_l^+, r_s^+)$       | $L = \pm L_\pm$      | $(r_l^+, r_\gamma^+)((r_s^+, r_\gamma^+))$ | $L = \pm L_+$   | $(r_l^+, r_\gamma^+)$ | $L = \pm L_\pm$ |
| $r = r_s^+$            | $L = \pm L_+; L = 0$ |  |                 | $r = r_\gamma^+$      | $L = \pm L_n$   |
| $(r_s^+, r_\gamma^+)$  | $L = \pm L_+$        |  |                 | $(r_\gamma^+, r_s^+)$ | $L = \pm L_-$   |
|                        |                      |  |                 | $r = r_s^+$           | $L = 0$         |
| Case VII               |                      | Case VIII                                  |                 | Case IX               |                 |
| Region                 | Momentum             | Region                                     | Momentum        | Region                | Momentum        |
| $r = r_l^+(r_s^+)$     | $\pm L_-$            | $r = r_l^+$                                | $L = 0$         | $r = r_s^+$           | $L = 0$         |
| $(r_l^+, r_s^+)$       | $L = \pm L_\pm$      | $(r_l^+, r_\gamma^+)$                      | $L = \pm L_+$   | $(r_s^+, r_\gamma^+)$ | $L = \pm L_+$   |
| $r = r_s^+$            | $L = 0$              | $r = r_\gamma^+$                           | $L = \pm L_n$   |                       |                 |

**Table 3.** Classification of the circular orbits of a charged test particle with charge-to-mass ratio  $\epsilon > 1$  in terms of the value of the ratio  $Q/M$  of a RN black hole.

| $Q/M \in (0, 1/2]$                         |             | $Q/M \in [1/2, \sqrt{13}/5)$               |             | $Q/M \in [\sqrt{13}/5, \sqrt{2}/3)$ |             | $Q/M \in [\sqrt{2}/3, 1)$                  |            |
|--|-------------|--|-------------|-------------------------------------|-------------|--|------------|
| Region                                     | Case        | Region                                     | Case        | Region                              | Case        | Region                                     | Case       |
| $1 < \epsilon \leq 2$                      | <i>I</i>    | $1 < \epsilon \leq M/Q$                    | <i>I</i>    | $1 < \epsilon \leq M/Q$             | <i>I</i>    | $1 < \epsilon \leq M/Q$                    | <i>I</i>   |
| $2 < \epsilon \leq M/Q$                    | <i>I</i>    | $M/Q < \epsilon \leq 2$                    | <i>II</i>   | $M/Q < \epsilon \leq \epsilon_n$    | <i>II</i>   | $M/Q < \epsilon \leq \epsilon_n$           | <i>II</i>  |
| $M/Q < \epsilon < \epsilon_n$              | <i>VI</i>   | $2 < \epsilon < \epsilon_n$                | <i>VI</i>   | $\epsilon = \epsilon_n$             | <i>III</i>  | $\epsilon = \epsilon_n$                    | <i>III</i> |
| $\epsilon = \epsilon_n$                    | <i>VII</i>  | $\epsilon = \epsilon_n$                    | <i>VII</i>  | $\epsilon_n < \epsilon \leq 2$      | <i>IV</i>   | $\epsilon_n < \epsilon < \tilde{\epsilon}$ | <i>IV</i>  |
| $\epsilon_n < \epsilon < \tilde{\epsilon}$ | <i>IV</i>   | $\epsilon_n < \epsilon < \tilde{\epsilon}$ | <i>IV</i>   | $2 < \epsilon < \tilde{\epsilon}$   | <i>IV</i>   | $\tilde{\epsilon} < \epsilon \leq 2$       | <i>V</i>   |
| $\epsilon = \tilde{\epsilon}$              | <i>VIII</i> | $\epsilon = \tilde{\epsilon}$              | <i>VIII</i> | $\epsilon = \tilde{\epsilon}$       | <i>VIII</i> | $\epsilon > 2$                             | <i>IX</i>  |
| $\epsilon > \tilde{\epsilon}$              | <i>IX</i>   | $\epsilon > \tilde{\epsilon}$              | <i>IX</i>   | $\epsilon > \tilde{\epsilon}$       | <i>IX</i>   |  |            |

ratio, we find four classes of objects characterized by

$$\text{I} : Q/M \in (0, 1/2], \quad (21)$$

$$\text{II} : Q/M \in (1/2, \sqrt{13}/5], \quad (22)$$

$$\text{III} : Q/M \in (\sqrt{13}/5, \sqrt{2}/3), \quad (23)$$

$$\text{IV} : Q/M \in ]\sqrt{2}/3, 1), \quad (24)$$

respectively. Thus, for a fixed charge of the spacetime, and following Table 3 and Table (2), we can trace a picture of the dynamical properties of that spacetime. An

**Table 4.** Classification in terms of the charge-to-mass ratio  $\epsilon > 1$  of the circular orbits of a charged test particle moving in the field of a RN black hole with mass  $M$  and charge  $Q$ .

| $1 < \epsilon \leq 2$   |            | $\epsilon > 2$          |             |
|-------------------------|------------|-------------------------|-------------|
| Region                  | Case       | Region                  | Case        |
| $0 < Q \leq M/\epsilon$ | <i>I</i>   | $0 < Q \leq M/\epsilon$ | <i>I</i>    |
| $M/\epsilon < Q < Q_n$  | <i>II</i>  | $M/\epsilon < Q < Q_n$  | <i>VI</i>   |
| $Q = Q_n$               | <i>III</i> | $Q = Q_n$               | <i>VII</i>  |
| $Q_n < Q < \tilde{Q}$   | <i>IV</i>  | $Q_n < Q < \tilde{Q}$   | <i>IV</i>   |
| $\tilde{Q} \leq Q < M$  | <i>V</i>   | $Q = \tilde{Q}$         | <i>VIII</i> |
|                         |            | $\tilde{Q} < Q < M$     | <i>IX</i>   |

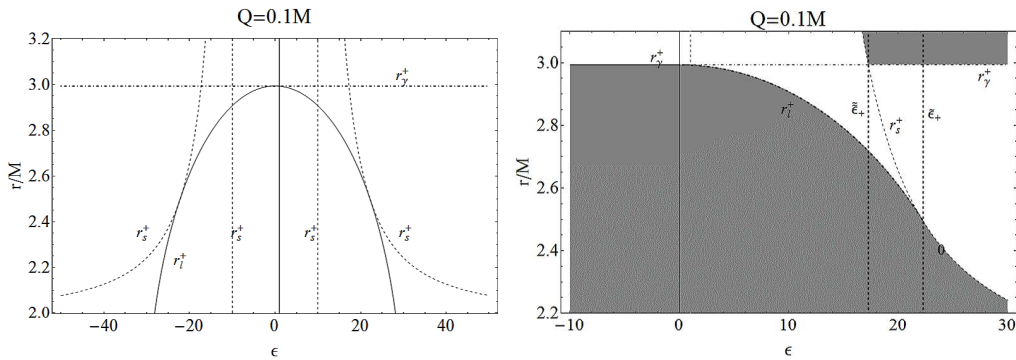


**Figure 3.** Black hole case with  $Q = 0.1M$ . Left panel: The radii  $r_s^+$ ,  $r_l^+$  and  $r_\gamma^+$  are plotted as functions of the test particle charge-to-mass ratio  $\epsilon$ . Shaded regions are forbidden (Right panel).

example is provided in figure 3 and figure 4, where the case of a spacetime of charge-to-mass ratio  $Q = 0.1M$  is illustrated. On the other hand, in Table 4, if we fix the charge-to-mass ratio of the test particle, and move towards increasing values of the charge-to-mass ratio of the source, we find only two different cases:  $\epsilon \leq 2$  and  $\epsilon > 2$ . Using this classification, we can determine the orbital radius followed by the selected particle in the fixed spacetime.

#### 4. Circular motion around a RN naked singularity

Equations (7) govern the circular motion around a RN naked singularity ( $Q \leq M$ ). Because (8) and (10) define the angular momentum  $L_\pm$  and the energy  $E_\pm$  in terms of  $r/M$ ,  $Q/M$ , and  $\epsilon$ , it is necessary to investigate several intervals of values. To this end, as in [15], it is useful to introduce the following notation

$$\epsilon_l \equiv \frac{\sqrt{9M^2 - 8Q^2}}{Q}, \quad (25)$$

$$\tilde{\epsilon}_\pm \equiv \frac{1}{\sqrt{2}Q} \sqrt{5M^2 \pm 4Q^2 + \sqrt{25M^2 - 24Q^2}}, \quad (26)$$

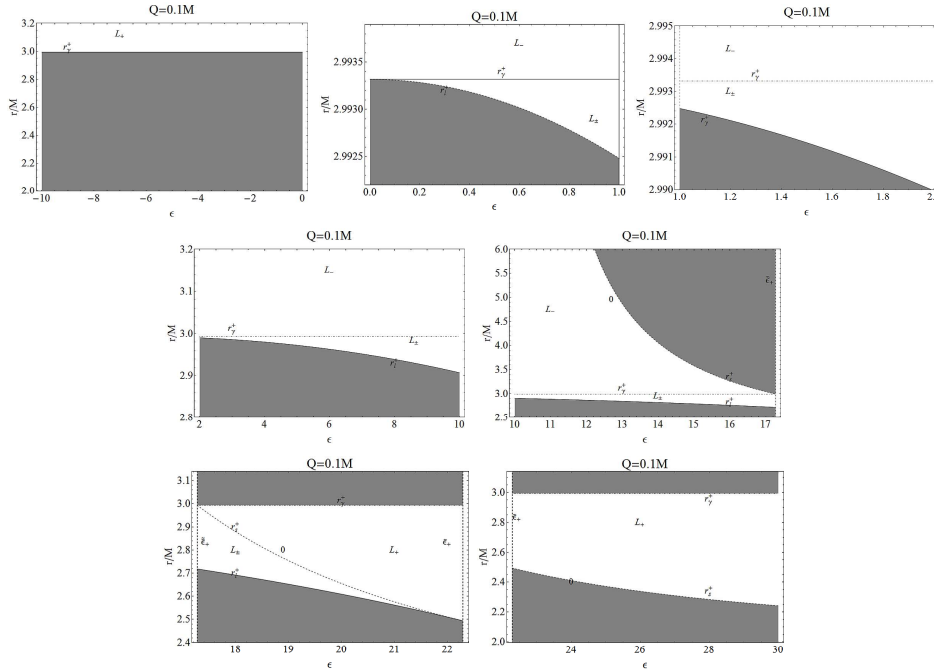


**Figure 4.** Black hole case with  $Q = 0.1M$ . Shaded regions are forbidden. The radii  $r_s^+$ ,  $r_l^+$  and  $r_\gamma^+$  are plotted as functions of the test particle charge-to-mass ratio  $\epsilon$  in the region  $[-10, 30]$ .

$$\tilde{\epsilon}_\pm \equiv \frac{1}{\sqrt{2}Q} \sqrt{3M^2 - 2Q^2 \pm M\sqrt{9M^2 - 8Q^2}}, \quad (27)$$

where  $\tilde{\epsilon}_- = \tilde{\epsilon}$  and  $\tilde{\epsilon}_+ = \epsilon_n$  as defined in (13) and (14), respectively. For completeness, and following [15], we reproduce here in figure 5 the behavior of these parameters in terms of the ratio  $Q/M > 1$ . It follows from figure 5 that it is necessary to consider the following four intervals:

$$\text{I} : Q/M \in (1, 5/(2\sqrt{6})], \quad (28)$$

$$\text{II} : Q/M \in (5/(2\sqrt{6}), (3\sqrt{6})/7), \quad (29)$$

$$\text{III} : Q/M \in ((3\sqrt{6})/7, \sqrt{9/8}), \quad (30)$$

$$\text{IV} : Q/M \in [\sqrt{9/8}, \infty). \quad (31)$$

This analysis completes the classification briefly presented in [15], and now contains all the different cases that are allowed by the values of  $\epsilon$ .

For  $\epsilon > 0$ , in general, circular orbits exist in the region  $r > r_* \equiv Q^2/M$ . In particular, for  $\epsilon > 1$  and  $M < Q < \sqrt{9/8}M$  circular orbits exist with angular momentum  $L = L_+$  in the interval  $r_\gamma^- < r < r_\gamma^+$ , while for  $Q \geq \sqrt{9/8}M$  no circular orbits exist [15]. The energy and angular momentum of circular orbits diverge as  $r$  approaches the limiting orbits at  $r_\gamma^\pm$ : the boundary  $r = r_\gamma^+$  in this case corresponds to a lightlike hypersurface. Finally, the energy of the states is always positive.

Since for  $\epsilon Q > 0$  the Coulomb interaction is repulsive, the situation characterized by the values for  $Q \geq \sqrt{9/8}M$  and  $\epsilon > 1$  corresponds to a repulsive electromagnetic effect that cannot be balanced by the attractive gravitational interaction.



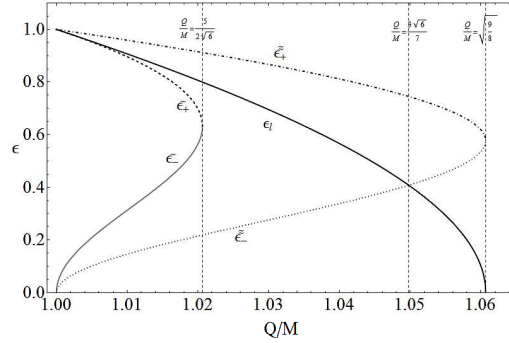


**Figure 5.** The charge parameters  $\epsilon_l$  (black solid curve),  $\tilde{\epsilon}_-$  (gray solid curve),  $\tilde{\epsilon}_+$  (dashed curve),  $\tilde{\tilde{\epsilon}}_-$  (dotted curve), and  $\tilde{\tilde{\epsilon}}_+$  (dotdashed curve) as functions of the charge-to-mass ratio of the RN naked singularity. The special lines  $Q/M = 5/(2\sqrt{6}) \approx 1.02$ ,  $Q/M = 3\sqrt{6}/7 \approx 1.05$ , and  $Q/M = \sqrt{9/8} \approx 1.06$  are also plotted.

For  $\epsilon < -1$ , the contribution of the electromagnetic interaction is always attractive. Hence, the repulsive force necessary to balance the attractive effects of the gravitational and Coulomb interactions can be generated only by the RN naked singularity. In particular, for  $\epsilon < -1$  and for  $Q > \sqrt{9/8}M$  circular orbits with  $L = L_+$  always exist for  $r > 0$ . For  $M < Q \leq \sqrt{9/8}M$ , circular orbits exist with  $L = L_+$  in  $0 < r < r_\gamma^-$  and  $r > r_\gamma^+$ . Charged test particles with  $\epsilon < -1$  can move along circular orbits also in the region  $(0, r_*]$ . The value of the energy on circular orbits increases as  $r$  approaches  $r = 0$ , and the angular momentum, as seen by an observer located at infinity, decreases as the radius of the orbit decreases. In the region  $M < Q \leq \sqrt{9/8}M$ , two limiting orbits appear at  $r_\gamma^\pm$  (similar to the neutral particle case [5]).

#### 4.1. Circular motion of particles with $0 < \epsilon < 1$ in a RN naked singularity

In this case, it is necessary to consider separately all the possible values of the charge parameters  $\epsilon_l$ ,  $\tilde{\epsilon}_\pm$  and  $\tilde{\tilde{\epsilon}}_\pm$  in all the regions given in (28-31) which, according to figure 5, follow for the values of the ratio  $Q/M$ .

In the first region,  $1 < Q/M \leq 5/(2\sqrt{6})$ , we analyze the energy and angular momentum of charged test particles for the following cases:

- (i)  $M < Q \leq 5/(2\sqrt{6})M$  and  $0 < \epsilon \leq \tilde{\tilde{\epsilon}}_-$ : See figure 6.
- (ii)  $M < Q \leq 5/(2\sqrt{6})M$  and  $\tilde{\tilde{\epsilon}}_- < \epsilon < \tilde{\epsilon}_-$ : See figure 7.
- (iii)  $M < Q \leq 5/(2\sqrt{6})M$  and  $\tilde{\epsilon}_- \leq \epsilon \leq \tilde{\epsilon}_+$ : See figure 8.
- (iv)  $M < Q \leq 5/(2\sqrt{6})M$  and  $\tilde{\epsilon}_+ < \epsilon \leq \epsilon_l$ : See figure 9.
- (v)  $M < Q \leq 5/(2\sqrt{6})M$  and  $\epsilon_l < \epsilon < \tilde{\tilde{\epsilon}}_+$ : See figure 10.
- (vi)  $M < Q \leq 5/(2\sqrt{6})M$  and  $\tilde{\tilde{\epsilon}}_+ \leq \epsilon < M/Q$ : See figure 11.
- (vii)  $M < Q \leq 5/(2\sqrt{6})M$  and  $M/Q \leq \epsilon < 1$ : See figure 12.

In the second interval,  $5/(2\sqrt{6}) < Q/M < (3\sqrt{6})/7$ , we analyze the energy and angular momentum of charged test particles for the following cases:

- (i)  $5/(2\sqrt{6})M < Q < (3\sqrt{6})/7M$  and  $0 < \epsilon < \tilde{\tilde{\epsilon}}_-$ : See figure 13.

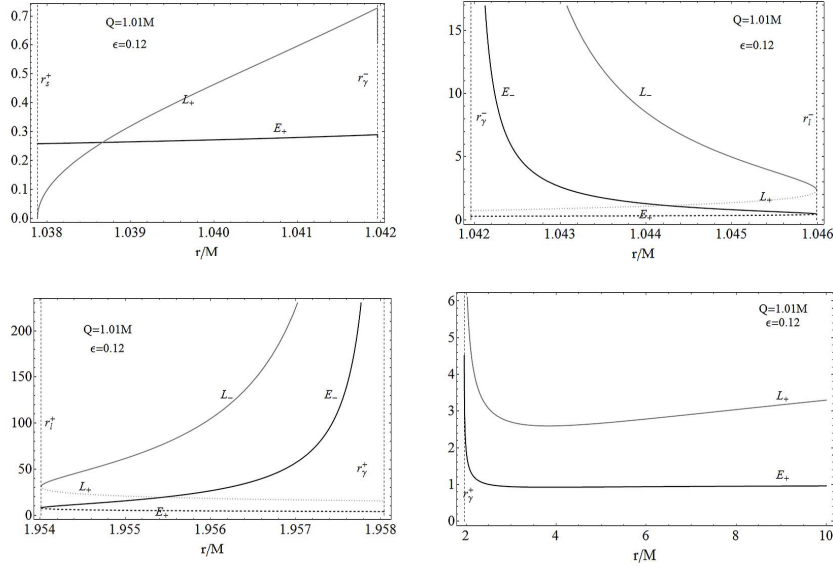


**Figure 6.** Case:  $M < Q \leq 5/(2\sqrt{6})M$  and  $0 < \epsilon \leq \tilde{\epsilon}_-$ . Parameter choice:  $Q = 1.01M$  and  $\epsilon = 0.12$ . Then  $\tilde{\epsilon}_- = 0.14639$ ,  $r_s^+ = 1.03789M$ ,  $r_\gamma^- = 1.04196M$ ,  $r_\gamma^+ = 1.95804M$ ,  $r_l^- = 1.04599M$ , and  $r_l^+ = 1.95401M$ . Circular orbits exist with angular momentum  $L = L^-$  (gray curve) and energy  $E = E^-$  (black curve) in  $r_s^+ < r < r_\gamma^-$ ;  $L = 0$  at  $r = r_s^+$  (upper left plot);  $L = L_\pm$  in  $r_\gamma^- < r \leq r_l^-$  (upper right plot) and in  $r_l^+ \leq r < r_\gamma^+$  (bottom left plot);  $L = L^-$  in  $r \geq r_\gamma^+$  (bottom right plot). The angular momentum  $L_+$  is represented by a gray dotted curve and the energy  $E_+$  by a black dashed curve.

- (ii)  $5/(2\sqrt{6})M < Q < (3\sqrt{6}/7)M$  and  $\tilde{\epsilon}_- < \epsilon < \epsilon_l$ : See figure 14.
- (iii)  $5/(2\sqrt{6})M < Q < (3\sqrt{6}/7)M$  and  $\epsilon_l \leq \epsilon \leq \tilde{\epsilon}_+$ : See figure 15.
- (iv)  $5/(2\sqrt{6})M < Q < (3\sqrt{6}/7)M$  and  $\tilde{\epsilon}_+ \leq \epsilon < M/Q$ : See figure 16.
- (v)  $5/(2\sqrt{6})M < Q < (3\sqrt{6}/7)M$  and  $M/Q \leq \epsilon < 1$ : See figure 17.

In the third interval,  $3\sqrt{6}/7 \leq Q/M \leq \sqrt{9/8}$ , we analyze the energy and angular momentum of charged test particles for the following cases:

- (i)  $(3\sqrt{6}/7)M \leq Q \leq \sqrt{9/8}M$  and  $0 < \epsilon \leq \epsilon_l$ : See figure 18.
- (ii)  $(3\sqrt{6}/7)M \leq Q \leq \sqrt{9/8}M$  and  $\epsilon_l < \epsilon \leq \tilde{\epsilon}_-$ : See figure 19.
- (iii)  $(3\sqrt{6}/7)M \leq Q \leq \sqrt{9/8}M$  and  $\tilde{\epsilon}_- < \epsilon < \tilde{\epsilon}_+$ : See figure 20.
- (iv)  $(3\sqrt{6}/7)M \leq Q \leq \sqrt{9/8}M$  and  $\tilde{\epsilon}_+ \leq \epsilon < M/Q$ : See figure 21.
- (v)  $(3\sqrt{6}/7)M \leq Q \leq \sqrt{9/8}M$  and  $M/Q \leq \epsilon < 1$ : See figure 22.

In the region  $Q > \sqrt{9/8}M$ , the only case in which circular orbits exist is for  $0 < \epsilon < M/Q$ . See figure 23. In general we can summarize the situation as follows.

There is always a minimum radius  $r_{min}$  at which circular motion is allowed. At the radius  $r_\gamma^-$  the energy of the test particle diverges, indicating that the hypersurface  $r = r_\gamma^-$  is lightlike. In the simplest case, there is a minimum radius  $r_{min}$  so that circular orbits are allowed in the infinite interval  $]r_{min}, \infty)$ . Otherwise, this region is split by a lightlike hypersurface situated at  $r_\gamma^+ > r_{min}$ .

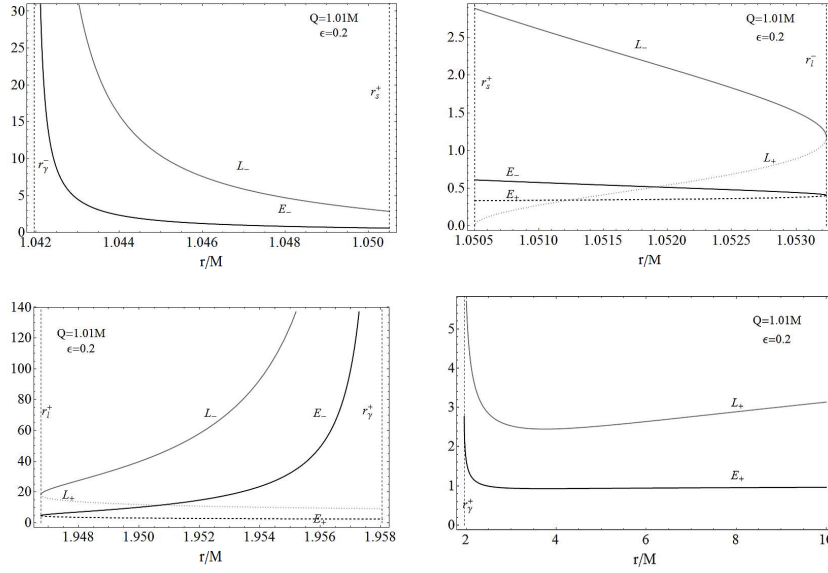


**Figure 7.** Case:  $M < Q \leq 5/(2\sqrt{6})M$  and  $\tilde{\epsilon}_- < \epsilon < \tilde{\epsilon}_-$ . Parameter choice:  $Q = 1.01M$  and  $\epsilon = 0.2$ . Then  $\tilde{\epsilon}_- = 0.14639$ ,  $\tilde{\epsilon}_+ = 0.313219$ ,  $r_s^+ = 1.0505M$ ,  $r_\gamma^- = 1.04196M$ ,  $r_\gamma^+ = 1.95804M$ ,  $r_l^- = 1.05323M$ , and  $r_l^+ = 1.94677M$ . Circular orbits exist with angular momentum  $L = L_+$  (gray curve) and energy  $E = E_+$  (black curve) in  $r_\gamma^- < r < r_s^+$  (upper left plot);  $L = L_\pm$  in  $r_s^+ \leq r < r_l^-$  (upper right plot) and  $r_l^+ \leq r < r_\gamma^+$  (bottom left plot);  $L = L^-$  in  $r \geq r_\gamma^+$  (bottom right plot). The angular momentum  $L^-$  (gray dotted curve) and the energy  $E^-$  (black dashed curve) are also plotted.

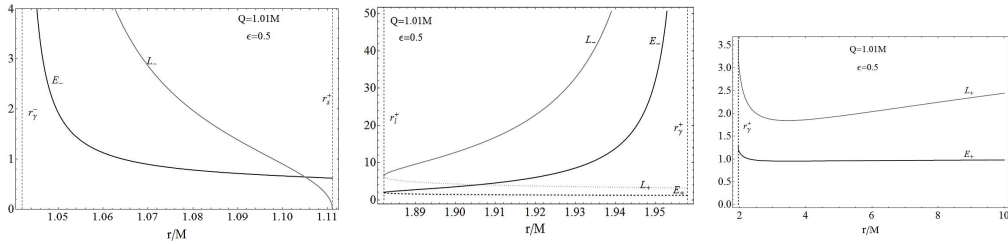


**Figure 8.** Case:  $M < Q \leq 5/(2\sqrt{6})M$  and  $\tilde{\epsilon}_- \leq \epsilon \leq \tilde{\epsilon}_+$ . Parameter choice:  $Q = 1.01M$  and  $\epsilon = 0.5$ . Then  $\tilde{\epsilon}_- = 0.313219$ ,  $\tilde{\epsilon}_+ = 0.896311$ ,  $r_s^+ = 1.11104M$ ,  $r_\gamma^- = 1.04196M$ ,  $r_\gamma^+ = 1.95804M$ ,  $r_l^- = 1.11784M$  and  $r_l^+ = 1.88216M$ . Circular orbits exist with angular momentum  $L = L_+$  (gray curve) and energy  $E = E_+$  (black curve) in  $r_\gamma^- < r < r_s^+$  (left plot);  $L = 0$  at  $r = r_s^+$ ;  $L = L_\pm$  in  $r_l^- \leq r < r_\gamma^+$  (center plot);  $L = L^-$  in  $r \geq r_\gamma^+$  (right plot).

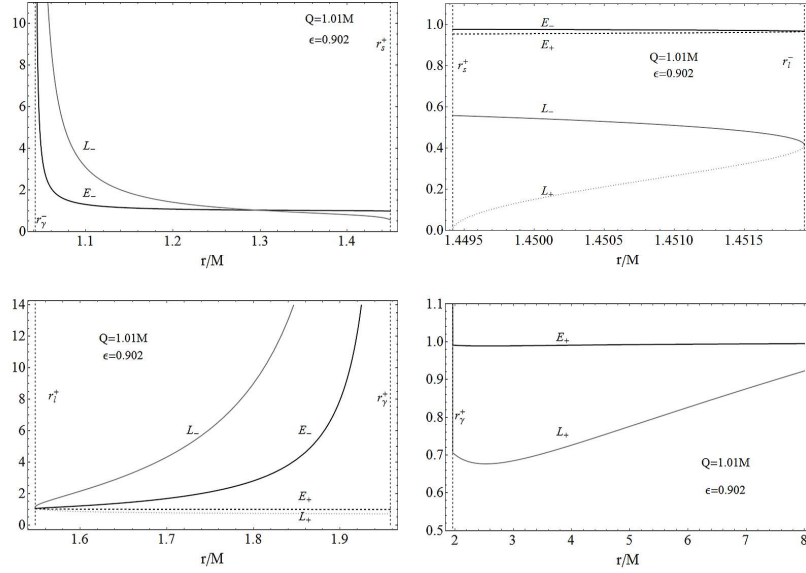


**Figure 9.** Case:  $M < Q \leq 5/(2\sqrt{6})M$  and  $\tilde{\epsilon}_+ < \epsilon \leq \epsilon_l$ . Parameter choice:  $Q = 1.01M$  and  $\epsilon = 0.902$ . Then  $\epsilon_l = 0.907$ ,  $\tilde{\epsilon}_+ = 0.8963$ ,  $r_s^+ = 1.44942M$ ,  $r_{\tilde{\gamma}}^- = 1.04196M$ ,  $r_{\tilde{\gamma}}^+ = 1.95804M$ ,  $r_l^- = 1.45192M$ , and  $r_l^+ = 1.548077M$ . Circular orbits exist with angular momentum  $L = L_+$  (gray curves) and energy  $E = E_+$  (black curves) in  $r_{\tilde{\gamma}}^- < r < r_s^+$  (upper left plot);  $L = L_{\pm}$  in  $r_s^+ \leq r < r_l^-$  (upper right plot) and  $r_l^+ \leq r < r_{\tilde{\gamma}}^+$  (bottom left plot);  $L = L^-$  in  $r \geq r_{\tilde{\gamma}}^+$  (bottom right plot).

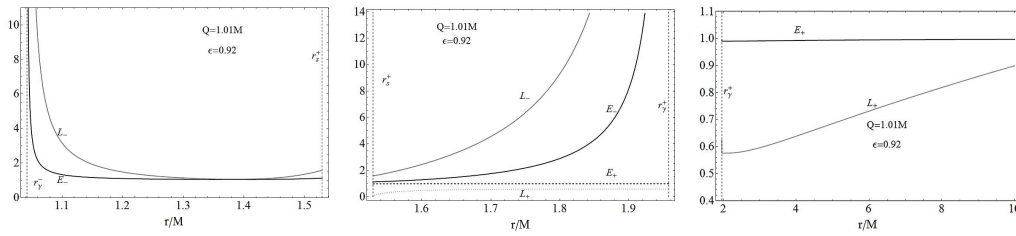


**Figure 10.** Case:  $M < Q \leq 5/(2\sqrt{6})M$  and  $\epsilon_l < \epsilon < \tilde{\epsilon}_+$ . Parameter choice:  $Q = 1.01M$  and  $\epsilon = 0.92$ . Then  $\epsilon_l = 0.907$ ,  $\tilde{\epsilon}_+ = 0.958884$ ,  $r_s^+ = 1.528942M$ ,  $r_{\tilde{\gamma}}^- = 1.04196M$ , and  $r_{\tilde{\gamma}}^+ = 1.95804M$ . Circular orbits exist with angular momentum  $L = L_+$  (gray curves) and energy  $E = E_+$  (black curves) in  $r_{\tilde{\gamma}}^- < r < r_s^+$  (left plot);  $L = L_{\pm}$  in  $r_s^+ \leq r < r_{\tilde{\gamma}}^+$  (center plot); and  $L = L^-$  in  $r \geq r_{\tilde{\gamma}}^+$  (right plot).

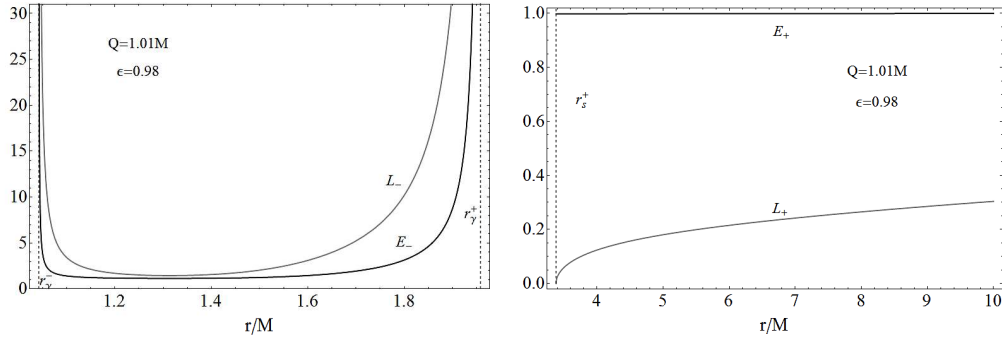


**Figure 11.** Case:  $M < Q \leq 5/(2\sqrt{6})M$  and  $\tilde{\epsilon}_+ \leq \epsilon < M/Q$ . Parameter choice:  $Q = 1.01M$  and  $\epsilon = 0.98$ . Then  $\tilde{\epsilon}_+ = 0.958884$ ,  $r_s^+ = 3.37999M$ ,  $r_\gamma^- = 1.04196M$ , and  $r_\gamma^+ = 1.95804M$ . Circular orbits exist with angular momentum  $L = L_+$  (gray curves) and energy  $E = E_+$  (black curves) in  $r_\gamma^- < r < r_\gamma^+$  (left plot) and  $L = L^-$  in  $r > r_s^+$  (right plot).

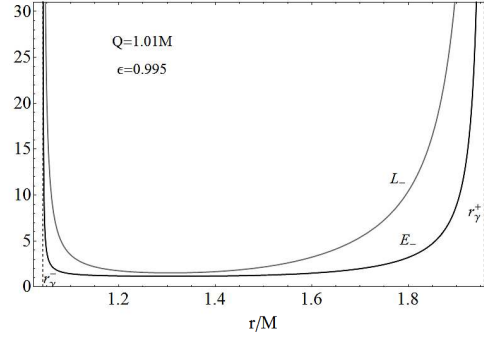


**Figure 12.** Case:  $M < Q \leq 5/(2\sqrt{6})M$  and  $M/Q \leq \epsilon < 1$ . Parameter choice:  $Q = 1.01M$  and  $\epsilon = 0.995$ . Then  $\tilde{\epsilon}_+ = 0.958884$ ,  $r_s^+ = 0.422853M$ ,  $r_\gamma^- = 1.04196M$ , and  $r_\gamma^+ = 1.95804M$ . Circular orbits exist with angular momentum  $l = L_+$  (gray curve) and energy  $E = E_+$  (black curve) in  $r_\gamma^- < r < r_\gamma^+$ .

Another possible structure is that of a spatial configuration formed by two separated regions in which circular motion is allowed in a finite region filled with charged particles within the spatial interval  $(r_{min} = r_\gamma^-, r_{max} = r_\gamma^+)$ . This region is usually surrounded by an empty finite region in which no motion is allowed. Outside the empty region, we find a zone of allowed circular motion in which either only neutral particles or neutral and charged particles can exist in circular motion.

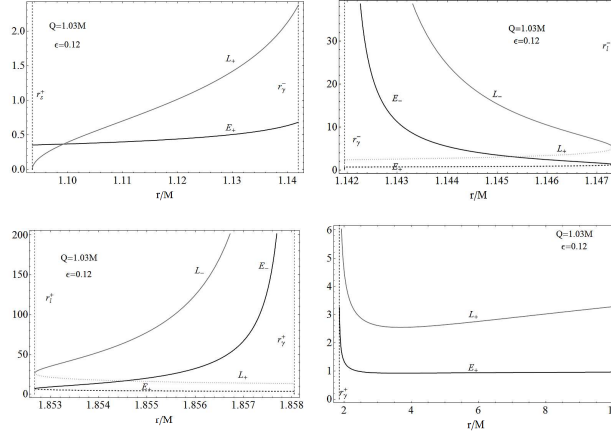


**Figure 13.** Case:  $5/(2\sqrt{6})M < Q < (3\sqrt{6}/7)M$  and  $0 < \epsilon < \tilde{\epsilon}_-$ . Parameter choice:  $Q = 1.03M$  and  $\epsilon = 0.12$ . Then  $\tilde{\epsilon}_- = 0.2772$ ,  $r_s^+ = 1.0935M$ ,  $r_\gamma^- = 1.1495M$ ,  $r_\gamma^+ = 1.858M$ ,  $r_l^- = 1.14732M$ , and  $r_l^+ = 1.8526804M$ . Circular orbits exist with angular momentum  $L = L^-$  (gray curves) and energy  $E = E^-$  (black curves) in  $r_s^+ < r \leq r_\gamma^-$  (upper left plot);  $L = 0$  at  $r = r_s^+$ ;  $L = L_\pm$  in  $r_\gamma^- < r \leq r_l^-$  (upper right plot) and  $r_l^+ \leq r < r_\gamma^+$  (bottom left plot);  $L = L^-$  in  $r \geq r_\gamma^+$  (bottom right plot).

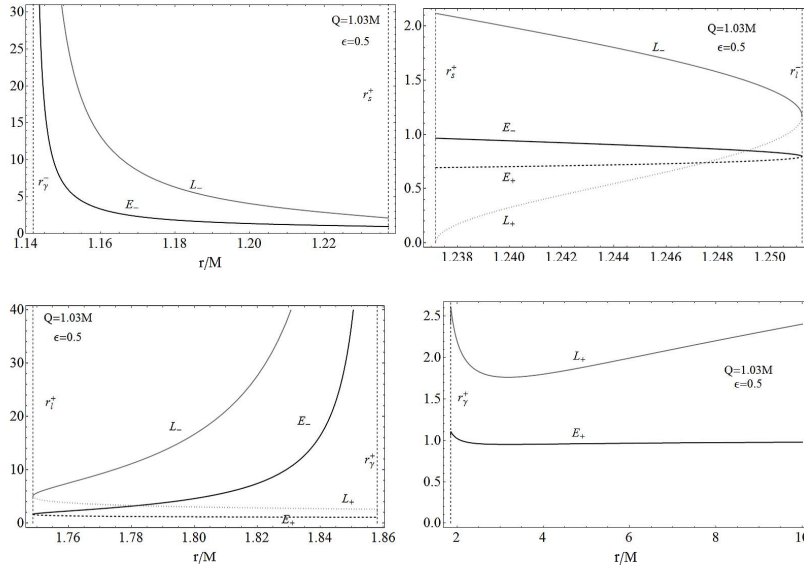


**Figure 14.** Case:  $5/(2\sqrt{6})M < Q < (3\sqrt{6}/7)M$  and  $\tilde{\epsilon}_- < \epsilon < \epsilon_l$ . Parameter choice:  $Q = 1.03M$  and  $\epsilon = 0.5$ . Then  $\tilde{\epsilon}_- = 0.2772$ ,  $\epsilon_l = 0.695243$ ,  $r_s^+ = 1.237M$ ,  $r_\gamma^- = 1.1495M$ ,  $r_\gamma^+ = 1.858M$ ,  $r_l^- = 1.25122M$ , and  $r_l^+ = 1.74878M$ . Circular orbits exist with angular momentum  $L = L_+$  (gray curve) and energy  $E = E_+$  (black curve) in  $r_\gamma^- < r < r_s^+$  (upper left plot);  $L = 0$  at  $r = r_s^+$ ;  $L = L_\pm$  in  $r_s^+ < r < r_l^-$  (upper right plot) and  $r_l^+ \leq r < r_\gamma^+$  (bottom left plot);  $L = L^-$  in  $r \geq r_\gamma^+$  (bottom right plot). (Reproduced from [15].)

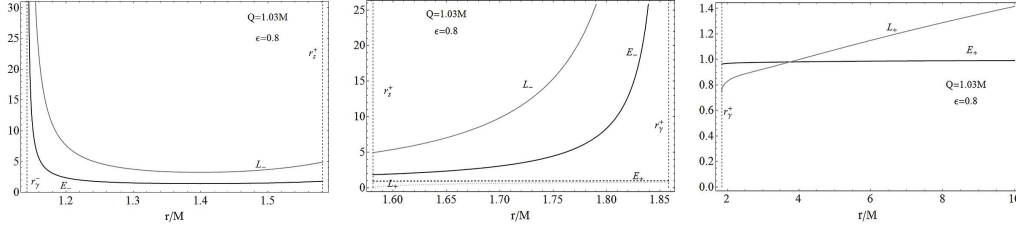


**Figure 15.** Case:  $5/(2\sqrt{6})M < Q < (3\sqrt{6}/7)M$  and  $\epsilon_l \leq \epsilon Q \leq \tilde{\epsilon}_+$ . Parameter choice:  $Q = 1.03M$  and  $\epsilon = 0.8$ . Then  $\tilde{\epsilon}_+ = 0.866828$  and  $\epsilon_l = 0.695243$ ,  $r_s^+ = 1.58116M$ ,  $r_{\gamma}^- = 1.1495M$ , and  $r_{\gamma}^+ = 1.858M$ . Circular orbits exist with angular momentum  $L = L_+$  (gray curve) and energy  $E = E_+$  (black curve) in  $r_{\gamma}^- < r < r_s^+$  (left plot);  $l = L_{\pm}$  in  $r_s^+ \leq r < r_{\gamma}^+$  (center plot); and  $L = L^-$  in  $r \geq r_{\gamma}^+$  (right plot).

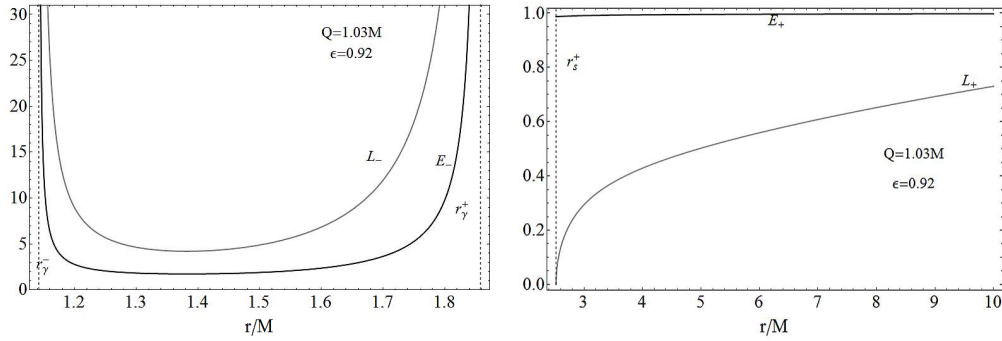


**Figure 16.** Case:  $5/(2\sqrt{6})M < Q < (3\sqrt{6}/7)M$  and  $\tilde{\epsilon}_+ \leq \epsilon < M/Q$ . Parameter choice:  $Q = 1.03M$  and  $\epsilon = 0.92$ . Then  $\tilde{\epsilon}_+ = 0.866828$ ,  $r_s^+ = 2.52M$ ,  $r_{\gamma}^- = 1.1495M$ , and  $r_{\gamma}^+ = 1.858M$ . Circular orbits exist with angular momentum  $L = L_+$  (gray curve) and energy  $E = E_+$  (black curve) in  $r_{\gamma}^- < r < r_{\gamma}^+$  (left plot) and  $L = L^-$  in  $r > r_s^+$ ;  $L = 0$  at  $r = r_s^+$  (right plot).

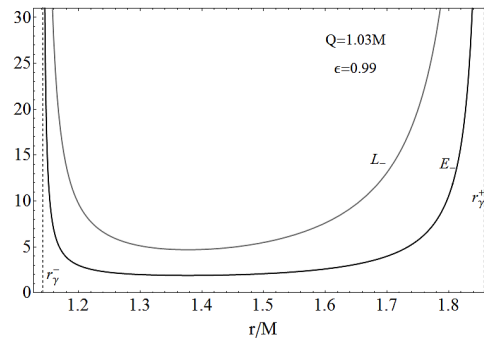


**Figure 17.** Case:  $5/(2\sqrt{6})M < Q < (3\sqrt{6}/7)M$  and  $M/Q \leq \epsilon Q < 1$ . Parameter choice:  $Q = 1.03M$  and  $\epsilon = 0.92$ . Then  $\tilde{\epsilon}_+ = 0.866828$ ,  $r_s^+ = 2.52M$ ,  $r_{\gamma}^- = 1.1495M$ , and  $r_{\gamma}^+ = 1.858M$ . Circular orbits exist with  $L = L_+$  (gray curve) and  $E = E_+$  (black curve) in  $r_{\gamma}^- < r < r_{\gamma}^+$ .

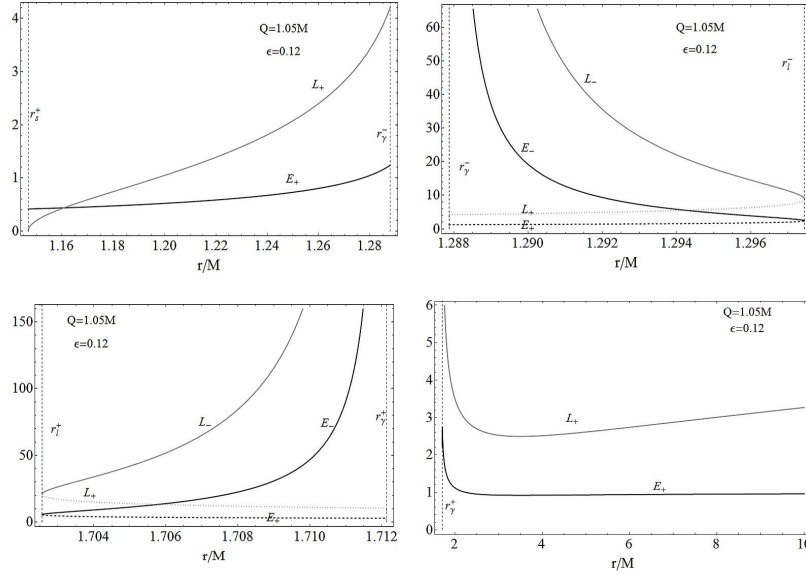


**Figure 18.** Case:  $(3\sqrt{6}/7)M \leq Q \leq \sqrt{9/8}M$  and  $0 < \epsilon \leq \epsilon_l$ . Parameter choice:  $Q = 1.05M$  and  $\epsilon = 0.12$ . Then  $\epsilon_l = 0.404$ ,  $r_s^+ = 1.1468M$ ,  $r_\gamma^- = 1.28787M$ ,  $r_l^+ = 1.71213M$ ,  $r_l^- = 1.29744M$ , and  $r_l^+ = 1.70256M$ . Circular orbits exist with angular momentum  $L = L^-$  (gray curve) and energy  $E = E^-$  (black curve) in  $r_\gamma^- \leq r \leq r_l^-$ ;  $L = 0$  at  $r = r_s^+$  (upper left plot);  $L = L_\pm$  in  $r_s^+ < r < r_l^-$  (upper right plot) and  $r_l^+ \leq r < r_\gamma^+$  (bottom left plot);  $L = L^-$  in  $r \geq r_\gamma^+$  (bottom right plot).

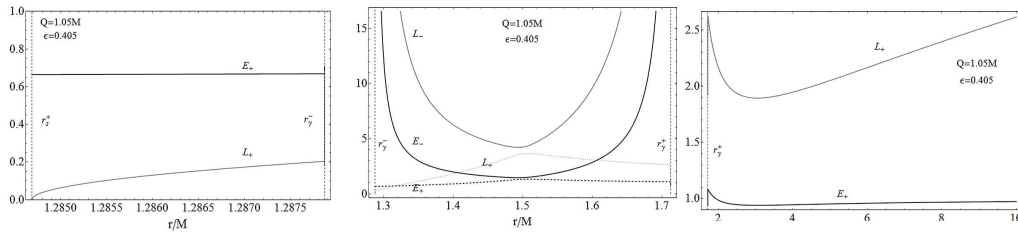


**Figure 19.** Case:  $(3\sqrt{6}/7)M \leq Q \leq \sqrt{9/8}M$  and  $\epsilon_l < \epsilon \leq \tilde{\epsilon}_-$ . Parameter choice:  $Q = 1.05M$  and  $\epsilon = 0.405$ . Then  $\epsilon_l = 0.404$ ,  $\tilde{\epsilon}_- = 0.41$ ,  $r_s^+ = 1.28M$ ,  $r_\gamma^- = 1.28787M$ , and  $r_\gamma^+ = 1.71213M$ . Circular orbits exist with angular momentum  $L = L^-$  (gray curve) and energy  $E = E^-$  (black curve) in  $r_s^+ < r < r_\gamma^-$ ;  $L = 0$  at  $r = r_s^+$  (left plot);  $L = L_\pm$  in  $r_\gamma^- \leq r < r_\gamma^+$  (center plot); and  $L = L^-$  in  $r \geq r_\gamma^+$  (right plot).



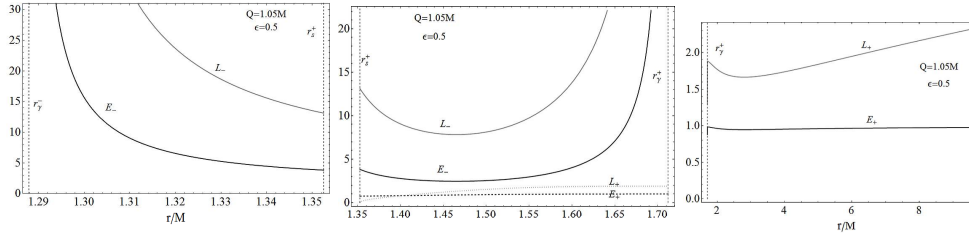


**Figure 20.** Case:  $(3\sqrt{6}/7)M \leq Q \leq \sqrt{9/8}M$  and  $\tilde{\epsilon}_- < \epsilon < \tilde{\epsilon}_+$ . Parameter choice:  $Q = 1.05M$  and  $\epsilon = 0.5$ . Then  $\tilde{\epsilon}_+ = 0.74$ ,  $\tilde{\epsilon}_- = 0.41$ ,  $r_s^+ = 1.35M$ ,  $r_{\gamma}^- = 1.28787M$ , and  $r_{\gamma}^+ = 1.71213M$ . Circular orbits exist with angular momentum  $L = L_+$  (gray curve) and energy  $E = E_+$  (black curve) in  $r_{\gamma}^- < r < r_s^+$  (left plot);  $L = L_{\pm}$  in  $r_s^+ \leq r < r_{\gamma}^+$  (center plot); and  $L = L_-$  in  $r \geq r_{\gamma}^+$  (right plot).

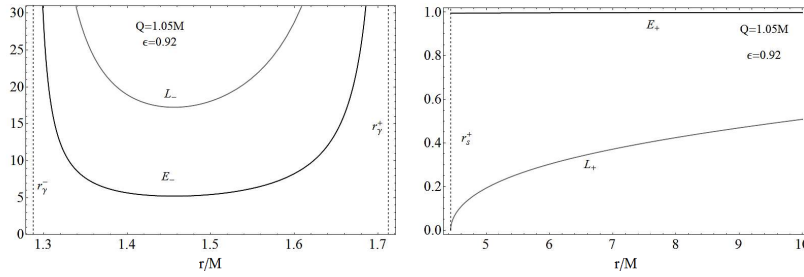


**Figure 21.** Case:  $(3\sqrt{6}/7)M \leq Q \leq \sqrt{9/8}M$  and  $\tilde{\epsilon}_+ \leq \epsilon < M/Q$ . choice:  $Q = 1.05M$  and  $\epsilon = 0.92$ . Then  $\tilde{\epsilon}_+ = 0.74$ ,  $r_s^+ = 4.437M$ ,  $r_{\gamma}^- = 1.28787M$ , and  $r_{\gamma}^+ = 1.71213M$ . Circular orbits exist with angular momentum  $L = L_+$  (gray curve) and energy  $E = E_+$  (black curve) in  $r_{\gamma}^- < r < r_{\gamma}^+$  (left plot) and  $L = L_-$  in  $r > r_s^+$ ;  $L = 0$  at  $r = r_s^+$  (right plot).

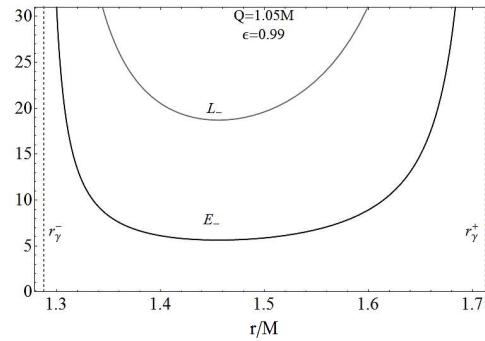


**Figure 22.** Case:  $(3\sqrt{6}/7)M \leq Q \leq \sqrt{9/8}M$  and  $M/Q \leq \epsilon < 1$ . Parameter choice:  $Q = 1.05M$  and  $\epsilon = 0.92$ . Then  $r_{\gamma}^- = 1.28787M$  and  $r_{\gamma}^+ = 1.71213M$ . Circular orbits exist with angular momentum  $L = L_+$  (gray curve) and energy  $E = E_+$  (black curve) in  $r_{\gamma}^- < r < r_{\gamma}^+$ .

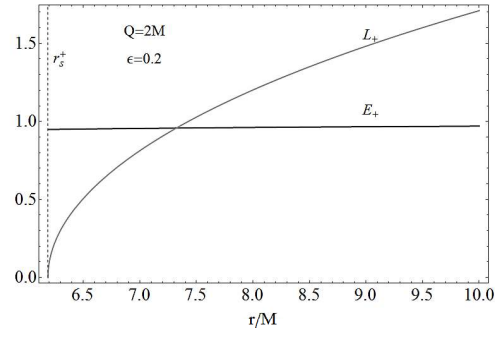


**Figure 23.** Case:  $0 < \epsilon < M/Q$  and  $Q > \sqrt{9/8}M$ . Parameter choice:  $Q = 2M$  and  $\epsilon = 0.2$ . Then  $r_s^+ = 6.18767M$ . Circular orbits exist with angular momentum  $L = L^-$  (gray curve) and energy  $E = E^-$  (black curve) in  $r > r_s^+$  and  $L = 0$  at  $r = r_s^+$ .

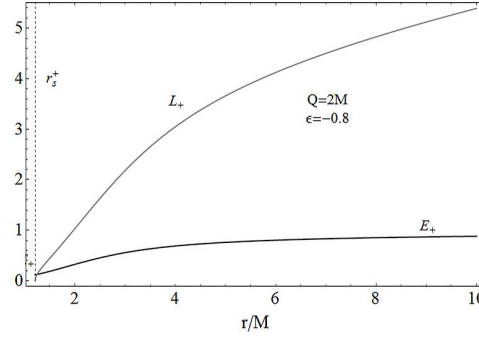


**Figure 24.** Case:  $Q > \sqrt{9/8}M$  and  $-1 < \epsilon < -M/Q$ . Parameter choice:  $Q = 2M$  and  $\epsilon = -0.8$ . Then  $r_s^+ = 1.2086M$ . Circular orbits exist with angular momentum  $L = L_+$  (gray curve) and energy  $E = E_+$  (black curve) in  $r > r_s^+$ . For  $r = r_s^+$ ,  $L = 0$ .

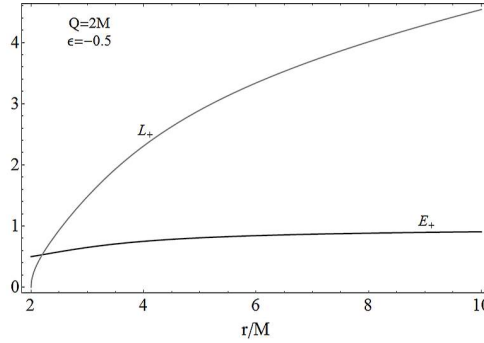


**Figure 25.** Case:  $Q > \sqrt{9/8}M$  and  $\epsilon = -M/Q$ . Parameter choice:  $Q = 2M$  and  $\epsilon = -0.5$ . Then  $r_s^+ = 1.2086M$ . Circular orbits exist with angular momentum  $L = L_+$  (gray curve) and energy  $E = E_+$  (black curve) in the region  $r > Q^2/(2M)$ . For  $r = Q^2/(2M)$ ,  $L = 0$ .

#### 4.2. Circular motion of particles with $-1 < \epsilon < 0$ in a RN naked singularity

For this range of values of the ratio  $\epsilon$ , we analyze the angular momentum and the energy in the following cases:

- (i)  $Q > \sqrt{9/8}M$  and  $-1 < \epsilon < -M/Q$ : See figure 24.
- (ii)  $Q > \sqrt{9/8}M$  and  $\epsilon = -M/Q$ : See figure 25.
- (iii)  $Q > \sqrt{9/8}M$  and  $-M/Q < \epsilon < 0$ : See figure 26.
- (iv)  $M < Q \leq \sqrt{9/8}M$  and  $-1 < \epsilon < -M/Q$ : See figure 27.
- (v)  $M < Q \leq \sqrt{9/8}M$  and  $\epsilon = -M/Q$ : See figure 28.
- (vi)  $M < Q \leq \sqrt{9/8}M$  and  $-M/Q < \epsilon < 0$ : See figure 29.

In general two different configurations are allowed. For  $Q > \sqrt{9/8}M$  a continuous region appears from a minimum radius  $r_{min} \in \{r_s^\pm, Q^2/(2M)\}$  to infinity in which circular orbits are allowed.

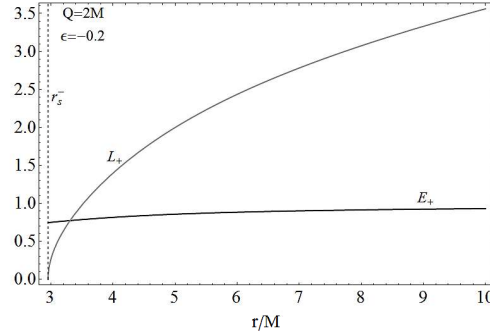


**Figure 26.** Case:  $Q > \sqrt{9/8}M$  and  $-M/Q < \epsilon < 0$ . Parameter choice:  $Q = 2M$  and  $\epsilon = -0.2$ . Then  $r_s^- = 2.9M$ . Circular orbits exist with angular momentum  $L = L_+$  (gray curve) and energy  $E = E_+$  (black curve) in  $r > r_s^-$ . For  $r = r_s^-$ ,  $L = 0$ .

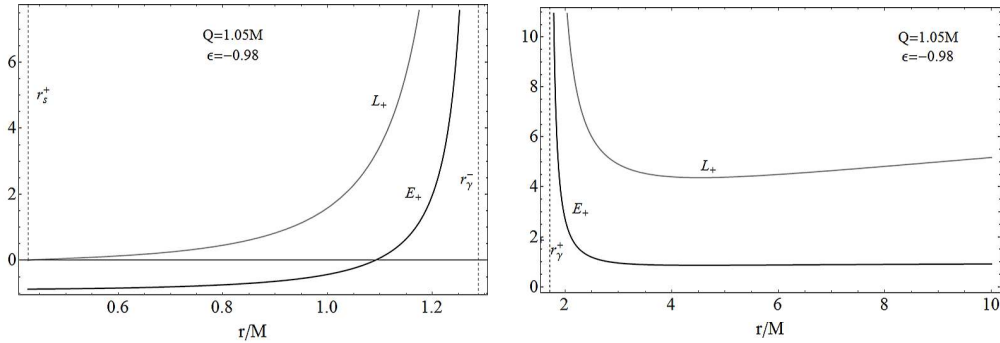


**Figure 27.** Case:  $M < Q \leq \sqrt{9/8}M$  and  $-1 < \epsilon < -M/Q$ . Parameter choice:  $Q = 1.05M$  and  $\epsilon = -0.98$ . Then  $r_s^+ = 0.427878M$ ,  $r_\gamma^- = 1.28787M$ , and  $r_\gamma^+ = 1.71213M$ . Circular orbits exist with angular momentum  $L = L_+$  (gray curve) and energy  $E = E_+$  (black curve) in  $r_s^+ < r < r_\gamma^-$  (left plot) and in  $r > r_\gamma^+$  for (right plot). For  $r = r_s^+$ ,  $L = 0$ . (Reproduced from [15].)

For  $M < Q \leq \sqrt{9/8}M$  there is a non connected region  $(r_{min}, \infty)$  inside which there is a forbidden region  $(r_\gamma^-, r_\gamma^+)$ . The configuration is therefore composed of two disconnected regions.

## 5. Conclusions

In this work, we explored the motion of charged test particles along circular orbits in the spacetime described by the Reissner–Nordström metric. A detailed discussion of the dynamics for the black hole and naked singularity cases has been performed. Circular orbits have been classified in detail for a complete set of cases.

We adopt the effective potential approach to study test particle orbits in the Reissner–Nordström spacetime, focusing on the equatorial orbits. We explore the morphology of the orbital regions. This analysis leads to a clear differentiation between naked singularities and black holes. A remarkable implication of this description is

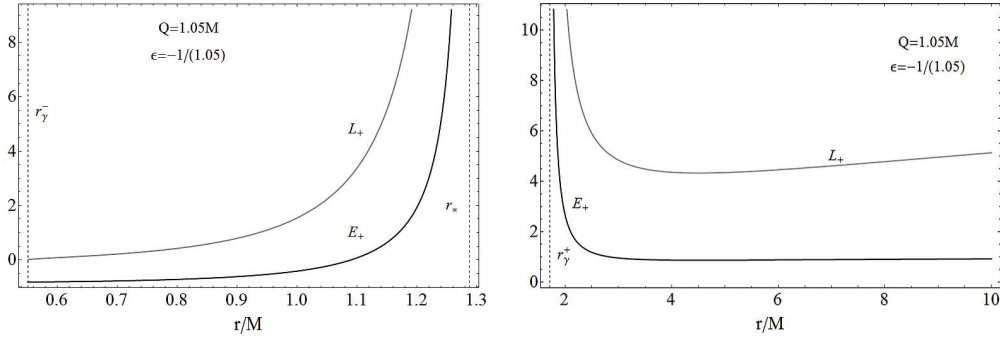


**Figure 28.** Case:  $M < Q \leq \sqrt{9/8}M$  and  $\epsilon = -M/Q$ . Parameter choice:  $Q = 1.05M$ . Then  $r_\gamma^- = 1.28787M$  and  $r_\gamma^+ = 1.71213M$ . Circular orbits exist with angular momentum  $L = L_+$  (gray curve) and energy  $E = E_+$  (black curve) in  $Q^2/(2M) < r < r_\gamma^-$  (left plot) and in  $r > r_\gamma^+$  (right plot). For  $r = Q^2/(2M)$ ,  $L = 0$ .

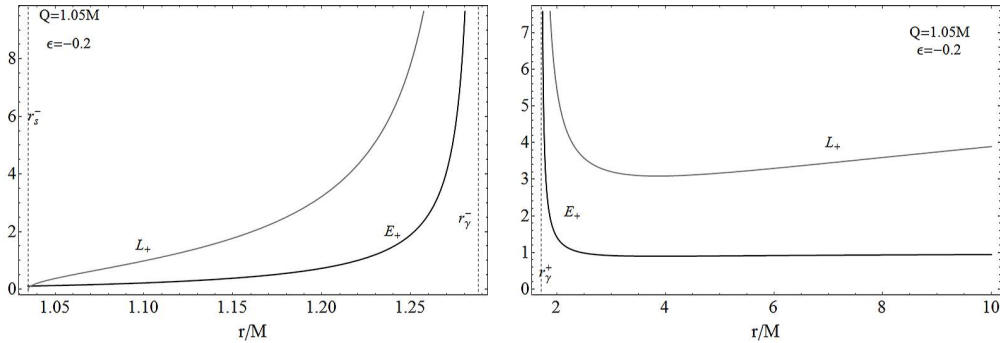


**Figure 29.** Case:  $M < Q \leq \sqrt{9/8}M$  and  $-M/Q < \epsilon < 0$ . Parameter choice:  $Q = 1.05M$  and  $\epsilon = -0.2$ . Then  $r_\gamma^- = 1.28787M$ ,  $r_\gamma^+ = 1.71213M$ , and  $r_s^- = 1.03487M$ . Circular orbits exist with angular momentum  $L = L_+$  (gray curve) and energy  $E = E_+$  (black curve) in  $r_s^- < r < r_\gamma^-$  (left plot) and in  $r > r_\gamma^+$  (right plot). For  $r = r_s^-$ ,  $L = 0$ .

that the circular orbit configuration in the black hole case is not allowed in the naked singularity regime. Instead, the study of the circular orbits trace out a possible way to distinguish the two physical situations.

In a series of previous works [5, 6, 15], we analyzed the dynamics of the RN spacetime, and studied the motion of neutral and charged test particles, by using the effective potential approach. We showed that in the case of charged test particles the term  $\epsilon Q/r$  drastically changes the behavior of the effective potential. The study shows the existence of stability regions whose geometric structure clearly distinguishes naked singularities from black holes (see also [16, 17] and [18, 19]). In [15], in particular, we studied the spatial regions of the RN spacetime where circular motion is allowed around either black holes or naked singularities. We showed that the geometric structure of stable accretion disks allows us to clearly distinguish between black holes and naked singularities. In this work, we presented the complete classification of

circular motion around a RN black hole, and around a RN naked singularity with  $0 < \epsilon < 1$  and  $-1 < \epsilon < 0$ .

Clearly, this analysis could be used to construct an accretion disk with disconnected rings made of test particles. A precise characterization of matter configurations surrounding a charged compact astrophysical object can account for significant astrophysical processes observed in the electromagnetic band, like the jet emissions. Therefore understanding the dynamics around compact objects is important for the understanding of the accretion disk phenomena and the classification of their general properties.

In the naked singularity case, gravity can assume a repulsive nature that produces a complicate picture of dynamics around the source. We distinguish four regions of charge-to-mass ratio values of the source that characterized these configurations. In each region, different cases can occur: an infinite, continuum, region or otherwise a disconnected region. In the black hole case the circular orbits configuration strongly varies if  $\epsilon \leq 1$  or  $\epsilon > 1$ . An infimum radius always appears, and in the case  $\epsilon > 1$  a supremum circular orbits radius can appear.

### Acknowledgments

One of us (DP) gratefully acknowledges financial support from the Blanceflor Boncompagni-Ludovisi née Bildt Foundation. This work was supported by CONACyT-Mexico, Grant No. 166391, by DGAPA-UNAM, and by CNPq-Brazil.

### References

- [1] Ruffini R 1972 *On the Energetics of Black Holes, Le Astres Occlus* (Les Houches)
- [2] Chandrasekhar S 1983 *The Mathematical Theory of Black Holes* (Clarendon Press, Oxford and Oxford University Press, New York)
- [3] Levin J and Perez-Giz G 2008 *Phys. Rev. D* **77** 103005
- [4] Bilic N 2006 *PoS P2GC* 004
- [5] Pugliese D and Quevedo H, Ruffini R 2011 *Phys. Rev. D* **83** 2
- [6] Pugliese D and Quevedo H and Ruffini R 2010 Circular motion in Reissner-Nordström spacetime *Preprint gr-qc/1003.2687*
- [7] Grunau S and Kagramanova V 2011 *Phys. Rev. D* **83** 044009
- [8] Bonnor W B 1993 *Class. Quantum Grav.* **10** 2077-2082
- [9] Bini D and Geralico A, Ruffini R 2007 *Phys. Rev. D* **75** 044012
- [10] Bini D and Geralico A, Ruffini R 2007 *Phys. Lett. A* **360** 515
- [11] Pradhan P and Majumdar P 2011 *Phys. Lett. A* **375** 474
- [12] Gladush V D and Galadgyi M V 2011 *Gen. Rel. Grav.* **43** 1347-1363
- [13] Cohen J M and Gautreau R 1979 *Phys. Rev. D* **19** 2273
- [14] Liang E P T 1974 *Phys. Rev. D* **9** 3257
- [15] Pugliese D and Quevedo H, Ruffini R 2011 *Phys. Rev. D* **83** 104052
- [16] Virbhadra K S and Ellis G F R 2002 *Phys. Rev. D* **65** 103004
- [17] Virbhadra K S and Keeton C R, *Phys. Rev. D* **77** (2008) 124014.
- [18] Dabrowski M P and Osarczuk J 1995 *Astroph. Space Sci.* **229** 139
- [19] Dabrowski M P and Prochnicka I 2002 *Phys. Rev. D* **66** 043508
- [20] Joshi P S 2007 *Gravitational Collapse and Spacetime Singularities* (Cambr. Univ. Press, Cambr.)
- [21] Joshi P S 2011 Key problems in black hole physics today *Preprint gr-qc/1104.3741*
- [22] Quevedo H 2011 *Int. J. Mod. Phys.* **20** 1779-1787
- [23] Dokuchaev V I 2011 *Class. Quant. Grav.* **28** 235015
- [24] Dotti G and Gleiser R, Pullin J 2007 *Phys. Lett. B* **644** 289
- [25] Patil M and Joshi P S, Kimura, Nakao M Ki 2012 *Phys. Rev. D* **86** 084023
- [26] Wunsch A, Muller T and Weiskopf D, Wunner G 2013 *Phys. Rev. D* **87** 024007

- [27] Balek V and Bicak J, Stuchlik Z 1989 *Bull. Astron. Inst. Czechosl* vol. 40 Publishing House of the Czechoslovak Academy of Sciences p. 133–165